Deviations from the impulse approximation in liquid ^{4}He: An experimental test at $Q=23$ Å^{-1}

T. R. Sosnick* and W. M. Snow†
Intense Pulsed Neutron Source, Argonne National Laboratory, Argonne, Illinois 60439

R. N. Silver
Theoretical Division and Los Alamos Neutron Scattering Center, Los Alamos National Laboratory, Los Alamos, New Mexico 87545

P. E. Sokol
Department of Physics, The Pennsylvania State University, University Park, Pennsylvania 16802
(Received 6 April 1990; revised manuscript received 9 August 1990)

Deep-inelastic-scattering measurements at high-momentum transfer Q can provide direct information on the momentum distribution of a system of particles if the impulse approximation (IA) is valid. In many such experiments, however, deviations between the observed scattering and predictions based on the IA are present. In liquid ^{4}He these deviations, called final-state effects (FSE), are caused by interactions among the particles. We have used liquid ^{4}He as a testing ground for the study of FSE. Deep-inelastic-neutron-scattering measurements on liquid ^{4}He have been carried out for temperatures of 0.35 and 3.5 K at a density of 0.147 g/cm^3. Under the assumption that current theoretical calculations of the momentum distribution of liquid ^{4}He are accurate, we extract the form of FSE in the superfluid phase from the scattering data. We also compare the predictions of several theories for FSE to the experimental data. At the momentum transfer of $Q=23$ Å^{-1} reached in these measurements, we find that an FSE theory due to Silver is the only current theory in agreement with the data in both the normal and superfluid phases.

I. INTRODUCTION

Deep-inelastic-scattering experiments are now performed in many fields of physics in an effort to gain information on momentum distributions.[1] The basic idea behind all such measurements is quite simple. In a deep-inelastic-scattering event, the energy and momentum transferred from the scattering probe to a particle in the target are very high compared to the characteristic energies and momenta of the particles in the system. In this limit the scattering law may be related to the momentum distribution through the impulse approximation (IA). Roughly speaking, the impulse approximation consists of the assumption that the scattering probe strikes a single particle of the target and that this particle recoils freely from the collision.

The scattering data exhibit an interesting scaling behavior as the energy and momentum transfer increases. In the case of neutron scattering from a monatomic system, for example, the dynamic structure factor $S(Q,\omega)$ is directly related to a Compton profile $J(Y,Q)$:

$$(Q/M)S(Q,\omega)\equiv J(Y,Q)\ , \tag{1.1}$$

$$Y\equiv\left[\frac{M}{Q}\right]\left[\omega-\frac{Q^2}{2M}\right]\ , \tag{1.2}$$

where ω and Q are the energy and momentum transfer from the neutron to the sample, and M is the mass of the scattering atom (we have chosen units in which $\hbar=1$). In the limit $Q\rightarrow\infty$, $J(Y,Q)$ tends to a function of Y only:

$$\lim_{Q\rightarrow\infty} J(Y,Q)\rightarrow J(Y)\ . \tag{1.3}$$

This behavior of the Compton profile is known as Y scaling.[2] If, in addition, the IA is valid, then Y is the component of the momentum along the direction of $\mathbf{Q}$, and $J_{\rm IA}(Y)$ is the longitudinal momentum distribution.

Deviations from the IA are present at finite values of Q. When such deviations exist, the momentum distribution cannot be inferred from the scattering data alone, and more information on the system becomes necessary. IA violations are typically understood to originate from two different classes of physical effects. In one class of effects, violations arise from the excitation of the internal degrees of freedom of the target particle. In this case, referred to as scale breaking, information on the internal excitations of the target is necessary in order to extract the momentum distribution. Deviations from the IA can also be caused by the interaction of the target particle with its environment. These deviations are generically called final-state effects (FSE's). In the presence of FSE's, the momentum distribution cannot be inferred without information on the interactions among the particles of the system.

Momentum distribution measurements provide the obvious practical reason for the interest in scaling violations. Less widely appreciated is the fact that scaling violations can be of interest in their own right. In the case of deep inelastic electron scattering from protons, for example, not only did the scaling behavior of the scattering data provide important evidence for the pres-

ence of quarks and gluons, but also the detailed form of the scaling *violations* was crucial experimental evidence for QCD as the theory of strong interactions.[3] In the case of deep inelastic neutron scattering from helium, FSE's are sensitive to nontrivial correlations in the strongly interacting ground state of the liquid. A correct description of FSE's in helium may provide important insight into the understanding of FSE's in a number of other dense, strongly interacting systems.

Liquid ^{4}He provides an excellent testing ground for the study of FSE's for several reasons. First of all, the helium atom does not possess any internal degrees of freedom which can be excited by neutron-nucleus scattering at the energies used to date in deep-inelastic-scattering experiments. Therefore, scale breaking cannot be the source of deviations from the IA, and only FSE's are relevant. In addition, many properties which are necessary for the theoretical calculation of FSE's, such as the helium-helium scattering cross section, the atomic density, and the pair-correlation function, have been measured accurately.

The most important information available on liquid ^{4}He, without which neither an experimental determination of FSE's nor a test of FSE theories could be conducted, comes from the extensive theoretical calculations of the momentum distribution. At zero temperature, calculations of the momentum distribution in the ground state of liquid ^{4}He have been performed using both variational methods and the Green's-function Monte Carlo (GFMC) method. At finite temperatures, the momentum distribution has been calculated using both finite temperature extensions of the variational calculations and the path-integral Mone Carlo (PIMC) method. Over the past few years, significant advances have been made in the sophistication of these methods. The results for many properties of liquid ^{4}He, such as the equation of state,[4] the static structure factor,[5] the elementary excitation spectrum,[6] and even the superfluid fraction,[7] are in good agreement with each other and with experiment. On the basis of this agreement, the calculations of the momentum distribution are expected to be quite accurate. Figure 1 shows the momentum distribution at $T=0$ K at a density of 0.147 g/cm^3 calculated using the GFMC method and the momentum distribution at $T=3.3$ K at a density of 0.138 g/cm^3 calculated using the PIMC method. We will assume that the results of the GFMC and PIMC calculations for $n(p)$ are also accurate in our experimental determination of FSE's and in the comparison of the scattering data to FSE theories.

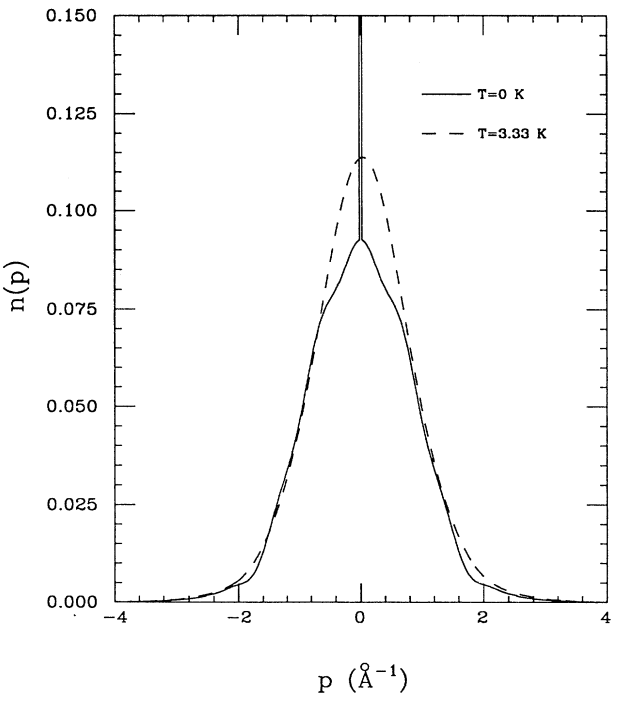

FIG. 1. Theoretical momentum distributions used in this paper to extract FSE's. The solid line is the GFMC (Ref. 4) result at $T=0$ K, which includes a δ-function singularity due to the condensate with 9.2% of the total intensity. The dashed line is the PIMC (Ref. 5) result in the normal liquid at $T=3.33$ K.

A unique characteristic of liquid ^{4}He which makes it ideal as a testing ground for FSE's is the presence of a δ-function singularity in its momentum distribution in the superfluid phase. This singularity is due to the presence of a Bose condensate containing approximately 9% of the atoms at $T=0$. In the absence of FSE's this singularity would be present in the observed scattering. In the presence of FSE's, the scattering in the superfluid phase is modified and provides a sensitive test of the details of FSE broadening. The presence of a condensate is especially important from this point of view because the width of the FSE broadening in liquid helium is small compared to the width of the nearly Gaussian momentum distribution of the noncondensate atoms. Without the condensate, an experimental extraction of FSE's from the scattering data would be much more difficult.

Finally, the momentum distribution of liquid ^{4}He has the unique property that the singular part of the momentum distribution, due to the condensate, can be turned off by entering the normal-liquid phase in which the condensate vanishes. The effect of FSE's on the normal-fluid scattering can provide an interesting contrast to the effects in the superfluid. For a large class of FSE theories in which the FSE broadening function in liquid ^{4}He is not expected to be very sensitive to temperature or even phase, the normal-fluid data can provide a nontrivial consistency check on the form of FSE's obtained from the superfluid data.

A quantitative understanding of FSE's in liquid ^{4}He would also enable a large body of inelastic-neutron-scattering experiments to be more fully understood. Previous measurements of the scattering from liquid helium for $Q<15$ Å^{-1} have exhibited significant deviations from the IA.[8–11] These deviations take the form of oscillations in the observed scattering of the peak center, width, and asymmetry of the line shape as a function of Q. The observed deviations are inconsistent with the minimum conditions which must be satisfied for the IA to be valid, and they show that FSE's are definitely present. The lack of understanding of FSE's in these measurements makes the extraction of information on the momentum distribu-

tion difficult. An understanding of the nature of FSE's at higher Q's, where the deviations from the IA are not as large, may lead to important progress in our understanding of the lower-Q data.

In this paper, we make use of recent high-resolution neutron-scattering studies of $S(Q,\omega)$ in liquid ^{4}He in both the normal and superfluid phases using much higher Q's than in previous high-resolution experiments. Under the assumption that the momentum distribution calculation by the GFMC method is accurate, we extract FSE's by comparing the predicted scattering obtained from the theoretical momentum distribution using the IA to the observed scattering in the superfluid phase. In addition, we compare several theories for FSE's to the observed scattering. Many of the theories provide a reasonable description of FSE's in the normal-liquid phase. However, we find that the only theory for FSE's which is consistent with the data in both the normal and superfluid phases at the Q's reached in our experiments is a recent theory due to Silver.[12]

This paper is organized as follows. Section II contains a discussion of deep inelastic neutron scattering. Section III covers experimental details. In Sec. IV we extract the form of final-state effects directly from the scattering data under the assumption that the theoretical calculations of the momentum distributions are correct. Section V presents comparisons of the scattering data to various theoretical treatments of final-state effects. We conclude in Sec. VI with a discussion of the significance of these comparisons and suggestions for future work.

II. DEEP INELASTIC NEUTRON SCATTERING

The scattering of neutrons is described by the double-differential scattering cross section

$$\frac{d^2\sigma}{d\Omega\, d\omega}=b^2\frac{k_f}{k_i}S(Q,\omega)\ , \tag{2.1}$$

where b is the neutron-nucleus scattering length for ^{4}He, $\mathbf{k}_i$ and $\mathbf{k}_f$ are the initial and final momenta of the scattered neutron, and $\mathbf{Q}$ and ω are the momentum and energy transfer from the neutron to the sample (we have chosen units in which $\hbar=1$). The dynamics of the sample are contained in $S(Q,\omega)$, the dynamic structure factor. The dynamic structure factor is directly proportional to the space and time Fourier transform of the equilibrium density-density correlation function.[13]

The density fluctuations which contribute to $S(Q,\omega)$ include both collective excitations involving many atoms and single-particle excitations. For sufficiently large Q, the distance $\sim 2\pi/Q$ over which the phase of the incident neutron changes significantly during the scattering process is small compared with the distance D between the scattering atoms. In this limit, known as the incoherent approximation, the part of $S(Q,\omega)$ due to the interference of scattering amplitudes from different atoms is negligible. The scattering is then due primarily to single-particle excitations. In the incoherent approximation, the expression for $S(Q,\omega)$ becomes

$$S(Q,\omega)\rightarrow S_{\rm inc}(Q,\omega)=\frac{1}{N}\int_{-\infty}^{+\infty}\exp(i\omega t)\sum_{j=1}^{n}\langle\exp[i\mathbf{Q}\cdot\mathbf{r}_j(0)]\exp[-i\mathbf{Q}\cdot\mathbf{r}_j(t)]\rangle dt\ , \tag{2.2}$$

where $\mathbf{r}_j(t)$ is the position vector of an atom and $\langle\cdots\rangle$ signifies a thermodynamic average. In liquid ^{4}He $2\pi/D\sim 2$ Å^{-1}. Measurements of the static structure factor $S(Q)$ show that it reaches the incoherent limit[14] for $Q>8$ Å^{-1}. In our experiments, Q at the center of the recoil peak is 23 Å^{-1}, and the incoherent approximation is certainly applicable.

The frequency moments of $S(Q,\omega)$ provide valuable information on the energy dependence of the scattering function for fixed Q. In general, they depend explicitly on the details of the interactions between the atoms. However, the first three moments of $S_{\rm inc}(Q,\omega)$ are independent of these details.[15] The moments are

$$M_0(Q)=\int S_{\rm inc}(Q,\omega)d\omega=1\ , \tag{2.3}$$

$$M_1(Q)=\int(\omega-\omega_r)S_{\rm inc}(Q,\omega)d\omega=0\ , \tag{2.4}$$

$$M_2(Q)=\int(\omega-\omega_r)^2S_{\rm inc}(Q,\omega)d\omega=\tfrac{4}{3}\omega_r\langle E_k\rangle\ , \tag{2.5}$$

where the recoil energy ω_r is $Q^2/2M_{\rm He}$ and $M_{\rm He}$ is the mass of the scattering atom. Under the conditions of the incoherent approximation, the average kinetic energy per atom, $\langle E_k\rangle$, can be obtained directly from the second moment of the observed scattering.

The scattering simplifies considerably in the limit $Q\rightarrow\infty$ if the interparticle interactions can be neglected. In this limit, known as the impulse approximation (IA), $S(Q,\omega)$ is directly related to the atomic momentum distribution $n(\mathbf{p})$:

$$\lim_{Q\rightarrow\infty}S(Q,\omega)=S_{\rm IA}(Q,\omega)=\frac{1}{\rho}\int n(\mathbf{p}_i)\delta(\omega-E(p_f)+E(p_i))\frac{d^3\mathbf{p}_i}{(2\pi)^3}\ , \tag{2.6}$$

where $\mathbf{p}_i$ is the initial momentum of an atom, $\mathbf{p}_f=\mathbf{p}_i+\mathbf{Q}$ is the final momentum of the recoilong atom, and $E(p)=p^2/2M_{\rm He}$ is its kinetic energy. The δ function in Eq. (2.6) represents the conservation of energy and momentum for the scattering of a neutron from a single atom. In the IA, the distance probed in the scattering event is much shorter than the typical distance traveled by a helium atom before it is significantly affected by in-

teractions with other atoms. The recoilong atoms then acts as a free particle during the collision.

Both the use of finite Q's and the presence of strong interactions between the particles can cause the IA to fail. In order to discuss the manner in which the IA is approached, it is convenient to express $S(Q,\omega)$ in terms of a Compton profile $J(Y,Q)$:

$$(Q/M_{\mathrm{He}})S(Q,\omega)\equiv J(Y,Q) , \tag{2.7}$$

$$Y\equiv\left[\frac{M_{\mathrm{He}}}{Q}\right]\left[\omega-\frac{Q^2}{2M_{\mathrm{He}}}\right] . \tag{2.8}$$

At this stage, this is just a formal transformation to a different set of independent variables. In terms of the Compton profile, the sum rules can be written in the form

$$\int_{-\infty}^{+\infty} J(Y,Q)dY=1 , \tag{2.9}$$

$$\int_{-\infty}^{+\infty} YJ(Y,Q)dY=0 , \tag{2.10}$$

$$\int_{-\infty}^{+\infty} Y^2J(Y,Q)dY=\tfrac{2}{3}M_{\mathrm{He}}\langle E_k\rangle . \tag{2.11}$$

The motivation for this transformation is the fact that, in the $Q\rightarrow\infty$ limit, the Compton profile is an isotropic system such as a liquid can be expressed[2] as a function of Y only:

$$\lim_{Q\rightarrow\infty} J(Y,Q)\rightarrow J(Y) . \tag{2.12}$$

This property of the Compton profile is called Y scaling. It is important to note that Y scaling alone does not imply the validity of the IA. Whether or not the IA is valid also depends on the nature of the interparticle interactions. For smooth interatomic potentials with Fourier transforms which decrease exponentially with Q, the IA is valid in the $Q\rightarrow\infty$ limit.[2] For atoms with infinitely repulsive hard-core interactions, however, $S(Q,\omega)$ obeys Y scaling in the $Q\rightarrow\infty$ limit, but the function of Y to which it scales is not directly related to $n(p)$.[16] Strictly speaking, of course, an infinitely repulsive hard-core interaction is unphysical. However, the interatomic forces in helium are steeply repulsive at short distances. As a result, a slow approach to the IA limit as a function of increasing Q is expected for helium.

In the IA, both Y and $J(Y)$ possess a direct physical meaning. Y is the component of the momentum along the direction of Q, and $J_{\mathrm{IA}}(Y)$ is the longitudinal momentum distribution. In this limit, $J_{\mathrm{IA}}(Y)$ is simply related to the momentum distribution:

$$J_{\mathrm{IA}}(Y)=\frac{1}{(2\pi)^2\rho}\int_{|Y|}^{+\infty} pn(p)dp$$

$$=\int_{-\infty}^{+\infty}\int_{-\infty}^{+\infty} n(p_x,p_y,Y)dp_xdp_y , \tag{2.13}$$

where the z axis is chosen to lie along the direction of Q. $J_{\mathrm{IA}}(Y)$ exhibits several features which are characteristic of the IA. It is symmetric about $Y=0$ and depends on Q only through the scaling variable Y. These features are equivalent to the more familiar conditions that $S(Q,\omega)$ satisfies in the IA. Namely, the scattering is centered at and is symmetric about the recoil energy ω_r, and the width of the scattering is directly proportional to Q and inversely proportional to M_{He}. In bulk liquid ^{4}He, both of these conditions are well satisfied[6] for Q's greater than 15 Å^{-1}.

For finite values of Q, neither the IA nor Y-scaling behavior is satisfied exactly. However, for sufficiently large Q, it is possible for the scattering data to exhibit Y scaling to a good approximation over a finite range of Q. In this case, an analysis of the data in terms of $J(Y)$ provides a more convenient framework for interpreting the results than an analysis using $S(Q,\omega)$. Figure 2 shows $J(Y,Q)$ in liquid ^{4}He for Q's of 7, 12 (Ref. 18), and 23 (Ref. 19) Å^{-1}. To a first approximation, the data from these different Q's fall on a universal curve $J(Y)$ and thus exhibit Y scaling. For this reason, in this paper we have chosen to perform the analysis in terms of $J(Y)$ instead of $S(Q,\omega)$.

The IA only approximately describes the scattering for currently accessible momentum transfers. Deviations from the IA, known as final-state effects (FSE's), result from the interaction of the recoiling helium atom with its neighbors during the scattering process. These interactions can alter the final momentum of the scattered neutron from the value expected in the IA based on energy and momentum conservation in the neutron-atom scattering.

Several theories of FSE's have been proposed. A detailed discussion of these theories is beyond the scope of this paper. However, for the purpose of comparing these theories to the experimental results, it is convenient to separate the theories into three classes: (a) broadening theories, (b) additive theories, and (c) theories with alter-

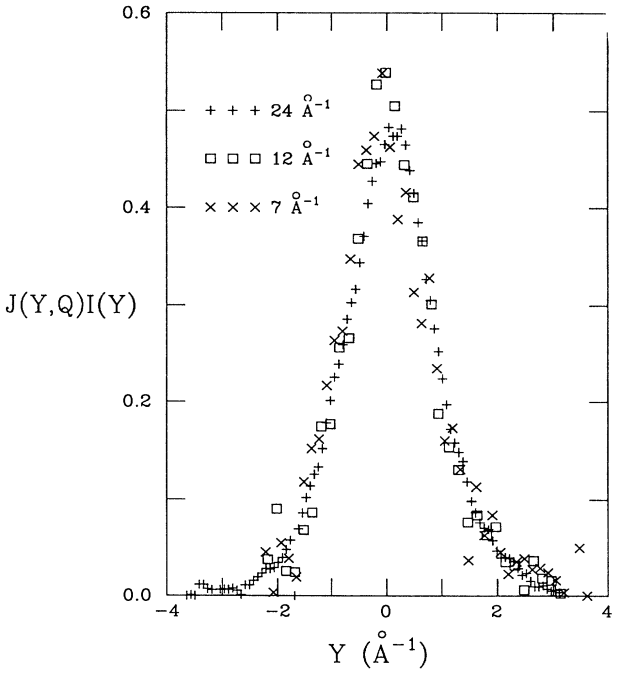

FIG. 2. Compton profile $J(Y,Q)$ for liquid ^{4}He at Q's of 7, 12, and 23 Å^{-1}. To a first approximation, all of the Compton profiles fall on a universal curve $J(Y)$ which is independent of Q.

native scaling variables.

In one class, referred to as broadening theories in this paper, the corrections to the IA are expressed as a convolution in Y space of the IA expression with a broadening function $R(Y,Q)$:

$$J(Y,Q)=\int_{-\infty}^{+\infty} R(Y-Y',Q)J_{\mathrm{IA}}(Y')dY' , \tag{2.14}$$

where $J_{\mathrm{IA}}(Y)$ satisfies the sum rules which are valid in the incoherent approximation. If the incoherent approximation is also valid for the experimental $J(Y,Q)$, then the sum rules place constraints on the shape of $R(Y,Q)$. The constraints are

$$\int_{-\infty}^{+\infty} R(Y,Q)dY=1 , \tag{2.15}$$

$$\int_{-\infty}^{+\infty} YR(Y,Q)dY=0 , \tag{2.16}$$

$$\int_{-\infty}^{+\infty} Y^2R(Y,Q)dY=0 . \tag{2.17}$$

To a first approximation, the convolution of a function with $R(Y,Q)$ simply broadens the function. However, since the first and second moment of $R(Y,Q)$ vanishes, $R(Y,Q)$ must possess both positive and negative values. As a result, a convolution also redistributes the intensity in a manner which cannot be viewed as a simple broadening. Whether or not this redistribution is a significant effect depends on the detailed form of $R(Y,Q)$.

Theoretical calculations of deviations from the IA have also been expressed as a sum of the IA result plus correction terms. For these theories, referred to as additive theories in this paper, it is common to split the correction terms into two parts:

$$J(Y,Q)=J_{\mathrm{IA}}(Y)+\Delta J_{\mathrm{sym}}(Y,Q)+\Delta J_{\mathrm{asym}}(Y,Q) , \tag{2.18}$$

where $\Delta J_{\mathrm{sym}}(Y,Q)$ and $\Delta J_{\mathrm{asym}}(Y,Q)$ are the FSE corrections which are symmetric and antisymmetric with respect to $Y=0$. Just as for $R(Y,Q)$, the first three sum rules for incoherent scattering place constraints on the symmetric and antisymmetric correction terms. These constraints are

$$\int_{-\infty}^{+\infty} \Delta J_{\mathrm{sym}}(Y,Q)dY=0 , \tag{2.19}$$

$$\int_{-\infty}^{+\infty} Y\Delta J_{\mathrm{asym}}(Y,Q)dY=0 , \tag{2.20}$$

$$\int_{-\infty}^{+\infty} Y^2\Delta J_{\mathrm{sym}}(Y,Q)dY=0 . \tag{2.21}$$

The sum rules constrain both the zeroth and second moments of $\Delta J_{\mathrm{sym}}(Y,Q)$ to vanish. From the zeroth-moment constraint, it follows that $\Delta J_{\mathrm{sym}}(Y,Q)$, if it is nonzero, must have both positive and negative values. This constraint, in combination with its symmetry about $Y=0$, forces $\Delta J_{\mathrm{sym}}(Y,Q)$ to possess at least three extrema as a function of Y.

The first-moment sum rule forces $\Delta J_{\mathrm{asym}}(Y,Q)$, if it is nonzero, to possess at least two maxima and two minima as a function of Y. By construction, $\Delta J_{\mathrm{asym}}(Y,Q)$ already has at least one maximum and one minimum. But if it has no other extrema, then $|Y\Delta J_{\mathrm{asym}}(Y,Q)|$ is necessarily positive everywhere, and its integral over limits which are symmetric about $Y=0$ can only vanish if $\Delta J_{\mathrm{asym}}(Y,Q)$ is zero.

III. EXPERIMENTAL DETAILS

This section contains a brief discussion of the experimental procedure used to obtain the scattering data and the methods of data analysis used to transform the scattering data to Y space. A more detailed discussion has appeared elsewhere.[20]

Inelastic-neutron-scattering measurements of liquid helium were carried out using the PHOENIX spectrometer at the Intense Pulsed Neutron Source (IPNS) at Argonne National Laboratory. PHOENIX is a time-of-flight inelastic spectrometer using a Fermi chopper for incident energy selection and a single high-angle detector bank ($135° < \theta < 144°$) containing 25 detectors for observation of the scattered neutrons. The incident energy used in these measurements of 495.5 meV corresponds to an average momentum transfer at the helium recoil peak of 23 Å^{-1}. The scattering from liquid helium was measured at temperatures of 0.35 and 3.5 K at a constant density of 0.147 g/cm^3. The helium sample was contained in a cylindrical sample cell made of 6061-T6 aluminum. The cell was 0.10 m high with an inner diameter of 0.04 m and a wall thickness of 1.6 mm. The cell was attached to the mixing chamber of a dilution refrigerator in a specially designed cryostat with no cryogens in the neutron beam. The cell temperature was monitored using germanium resistance thermometers attached to the top and bottom of the cell.

The scattered neutrons are histogrammed as a function of time of flight for each detector individually. The data from each detector are transformed to $S(Q,\omega)$ using the mean incident energy and time at sample obtained by comparing a Monte Carlo simulation of the incident beam with the observed monitor spectra. The data are then converted to $J(Y)$ using the energy and momentum transfer for each histogrammed point and the known mass of the helium atom. Finally, in order to take into account any systematic errors in the Y scale, the scattering data are shifted by $+0.04$ Å^{-1} (about half a channel width) so that the first-moment sum rule for incoherent scattering is satisfied.

Since the statistical accuracy of the results from an individual detector is low, the data from the 25 detectors are added together after being converted to a common Y scale. There is little variation of Q across the detector bank and the data that are already approximately Y scale, and so this procedure results in a significant increase in the statistical accuracy of the results with little degradation in instrumental resolution.

An absolute-intensity scale for the scattering was obtained from measurements of low-density (0.0073 g/cm^3) helium gas at 5.6 K using the same experimental setup and cell as used in the liquid measurements. This provides an absolute-intensity scale to within the 5% statistical uncertainty in determining the area of the helium peak. Thus, after correcting for the effects of sample self-shielding and multiple scattering, the scattering from the liquid may be placed on an absolute-intensity scale.

The effects of instrumental resolution must be taken into account in order to determine the true scattering from the liquid. In general, the instrumental broadening

is a complicated function depending on the energy and momentum transfer and the instrument geometry, and a simple closed-form expression for the resolution function is not possible. In the case of helium, for which the bulk of the scattering intensity is concentrated near $Y=0$, an effective resolution function which is a simple one-dimensional convolution can be defined. This effective resolution function, $I(Y,Q)$, is calculated by a Monte Carlo simulation of the spectrometer. In terms of $I(Y,Q)$, the observed resolution-broadened Compton profile $J_{\rm obs}(Y,Q)$ is

$$J_{\rm obs}(Y,Q)=\int_{-\infty}^{+\infty} I(Y-Y',Q)J(Y',Q)dY' , \qquad (3.1)$$

where $J(Y,Q)$ is the unbroadened Compton profile. The instrumental broadening has a full width at half maximum (FWHM) of ~ 0.6 Å^{-1} and is much narrower than the total observed scattering.

IV. EXPERIMENTAL DETERMINATION OF FSE CORRECTIONS

The observed scattering from the bulk liquid at temperatures of 0.35 and 3.5 K and at a constant density of 0.147 g/cm^3 is shown in Figs. 3(a) and 3(b). The scattering has been converted to an absolute-intensity scale using the helium-gas measurements. The integrated intensity of the observed scattering, when sample attenuation is taken into account, is unity at all the temperatures, to within the 5% error in the absolute-intensity scale provided by the helium-gas measurement. Thus the observed scattering satisfies the zeroth-moment sum rule for incoherent scattering, which simply indicates that all the scattering is observed. In addition, the observed scattering is consistent with the minimal features mentioned in Sec. II for IA scattering.

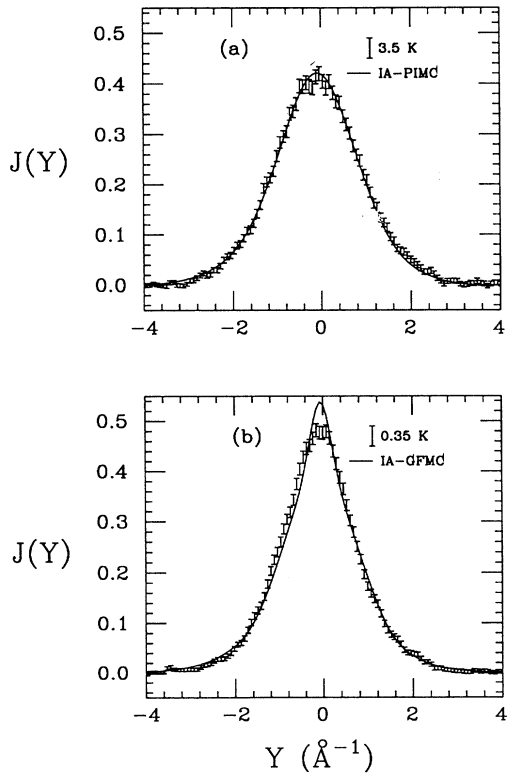

FIG. 3. (a) Normal-liquid data at $T=3.5$ K. The line is the instrumentally broadened IA prediction using the PIMC calculation of $n(p)$. (b) Superfluid data at $T=0.35$ K. The line is the instrumentally broadened IA prediction using the GFMC calculation of $n(p)$.

We will now exhibit the presence of final-state effects in the scattering data under the assumption that the theoretical calculations of the momentum distributions are accurate. We will use the IA to convert the theoretical $n(p)$ to $J_{\rm IA}(Y)$, broaden $J_{\rm IA}(Y)$ by the instrumental resolution function, and compare the result directly to the scattering data. If the momentum distribution calculations are correct, then any differences which appear in this comparison must be due to FSE's.

Figure 3(a) shows a comparison between the observed scattering in the normal liquid at 3.5 K and a density of 0.147 g/cm^3 and the theoretical prediction of the PIMC results of Ceperley and Pollock[5] at 3.33 K and a slightly lower density of 0.138 g/cm^3. The theoretical prediction has been converted to $J_{\rm IA}(Y)$ using the IA and broadened by the instrumental resolution. The agreement between the IA prediction and the observed scattering is excellent. Deviations from the IA due to FSE's are very small in the normal-liquid scattering at these Q's.

Figure 3(b) shows a similar comparison of the experimental results at 0.35 K and the ground-state GFMC calculation of Whitlock and Panoff[4] at the same density. Differences between the theoretical prediction and experimental results are clearly evident. The GFMC calculation predicts substantially higher intensity near the peak center than the experimental results. This discrepancy is just what one would expect if a condensate peak is present which is broadened by FSE's.

If the FSE's are expressed as a convolution with the IA prediction, as in Eq. (2.14), then the final-state broadening function may be obtained by deconvoluting the instrumental resolution function and $J_{\rm IA}(Y)$ from the observed scattering. The dotted line in Fig. 4 shows the result of this deconvolution for the superfluid data. The experimentally determined $R(Y,Q)$ exhibits a sharp central peak and negative tails at higher Y. Figure 4 also shows the shape of $R(Y,Q)$ for some of the broadening theories which will be discussed in Sec. V.

There are two noteworthy features in the experimentally determined $R(Y,Q)$. First of all, the $R(Y,Q)$ obtained from the deconvolution satisfies the constraints which follow from the sum rules for incoherent scattering within the uncertainties of the deconvolution procedure. This must be true in the incoherent approximation, since in this case both $J(Y,Q)$ and $J_{\rm IA}(Y)$ obey the second-moment sum rule. In particular, as mentioned in Sec. II, the negative tails are consistent with the second-moment sum rule. In addition, the central peak of the broadening function is relatively narrow with a full FWHM of 0.67 Å^{-1}.

While the general features of the extracted $R(Y,Q)$ are accurate, the finer details of the shape are affected by the

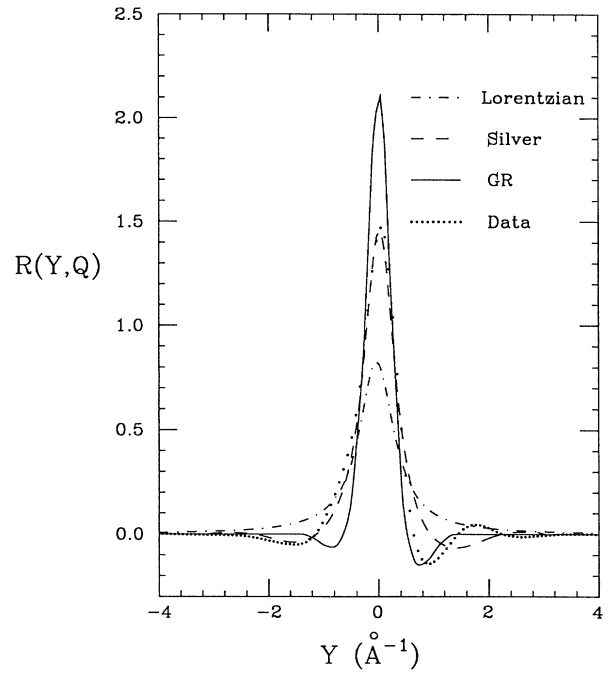

FIG. 4. Comparison of the experimentally determined FSE broadening function $R(Y,Q)$ in the superfluid phase with various theories. The dot-dashed line is the Lorentzian broadening function with a width $\Gamma=\rho\sigma(Q)/2$. The dashed line is the broadening function due to Silver. The solid line is the broadening function due to Gersch and Rodriguez. The dotted line is the broadening function determined from the experimental data in the superfluid phase.

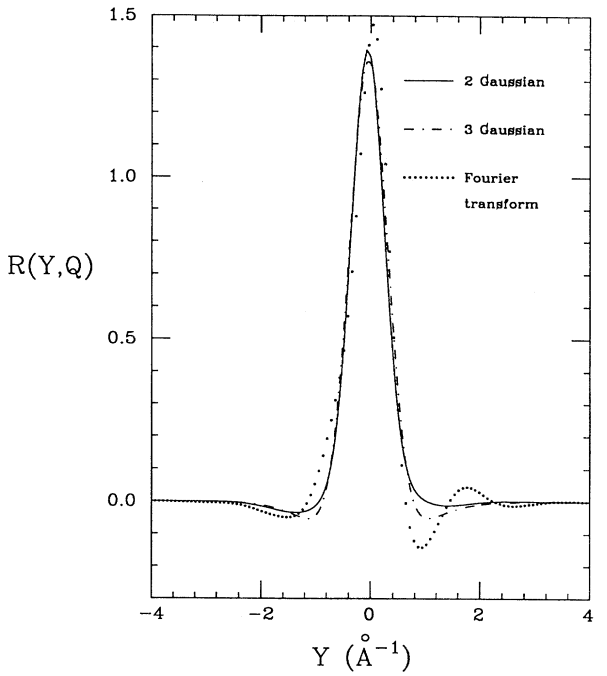

FIG. 5. Three different $R(Y,Q)$'s which produce equally good fits to the experimental data when convoluted with the instrumental resolution function and the GFMC $J_{IA}(Y)$. The dotted line is $R(Y,Q)$, as determined from a Fourier transform deconvolution. The solid line is $R(Y,Q)$, as determined from a fit using a parametrized two-Gaussian form. The dot-dashed line is $R(Y,Q)$, as determined from a fit using a parametrized three-Gaussian form.

statistical noise in the numerical deconvolution procedure. To illustrate which features of $R(Y,Q)$ are determined by the scattering data, we have performed deconvolutions in which the form of $R(Y,Q)$ is constrained to be a sum of Gaussians. Figure 5 shows the results of the numerical deconvolution shown in Fig. 4 along with two Gaussian and three Gaussian $R(Y,Q)$'s. Upon convolution with the instrumental resolution function and the GFMC $J_{IA}(Y)$, all of the $R(Y,Q)$'s shown in Fig. 5 produce equally good agreement with the experimental data. It is clear from Fig. 5 that the main feature of the FSE broadening function which is constrained by the data is its width. The detailed features of $R(Y,Q)$ at high $|Y|$ cannot be determined from our scattering data.

Although all of the results of this paper are obtained under the assumption that the theoretical calculations of the momentum distributions are accurate, it is useful to possess a qualitative understanding of the sensitivity of the extracted $R(Y,Q)$ to certain features of the underlying momentum distribution. We have performed two sensitivity tests. In the first test, we have compared the extracted $R(Y,Q)$'s obtained from two momentum distributions with the same condensate fraction, but with different distributions for the uncondensed atoms. Figure 6(a) shows the GFMC $J_{IA}(Y)$ along with a Gaussian $J_{IA}(Y)$ with the same kinetic energy (14.5 K) and the same value for the condensate fraction (9.2%). There are differences between the two momentum distributions at low Y and at high Y. Nevertheless, the corresponding two Gaussian $R(Y,Q)$'s, shown in Fig. 6(b), are similar in width. In the second test, we have compared the extracted $R(Y,Q)$'s obtained from three momentum distributions with the same functional form for the uncondensed momentum distribution, but with different condensate fractions. Figure 6(c) shows three Gaussian $J_{IA}(Y)$'s with the same kinetic energy as in Fig. 6(a), but with condensate fractions of 7%, 9%, and 11%. The extracted $R(Y,Q)$'s are shown in Fig. 6(d). There are large differences between the $R(Y,Q)$ extracted from the momentum distribution with a 7% condensate and the other two extracted $R(Y,Q)$'s. As one might expect, the width of the extracted $R(Y,Q)$ is somewhat more sensitive to changes in the size of the condensate than it is to changes in the momentum distribution of the uncondensed atoms.

Another feature of the momentum distribution of the uncondensed atoms which might be expected to affect the extracted $R(Y,Q)$ is the condensate-induced power-law singularity which is expected on theoretical grounds.[21–26] This term is included in the $T=0$ momentum distribution calculation of Manousakis and Pandharipande,[6] and the calculated $n(p)$ shows significant

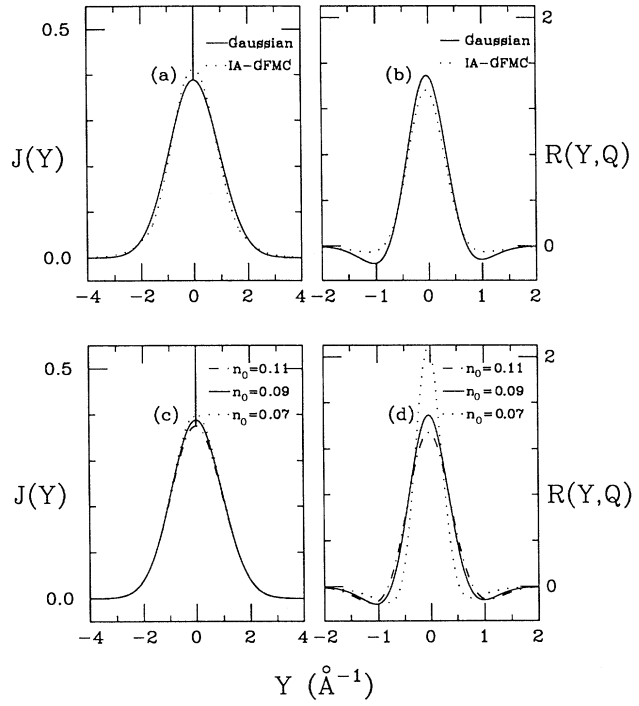

FIG. 6. Sensitivity of the extracted $R(Y,Q)$ to certain features of the underlying longitudinal momentum distribution. (a) GFMC momentum distribution along with a Gaussian momentum distribution with the same condensate fraction of 9.2% and the same kinetic energy of 14.5 K. (b) Corresponding $R(Y,Q)$'s as determined from a fit using a parametrized two-Gaussian form. (c) Three-Gaussian momentum distributions with the same kinetic energy of 14.5 K with condensate fractions of 7%, 9%, and 11%. (d) Corresponding $R(Y,Q)$'s.

differences from the GFMC momentum distribution at small p. However, these differences become very small when the three-dimensional momentum distribution $n(p)$ is converted to the longitudinal momentum distribution $J(Y)$.[27] This is because $J(Y)$ is proportional to the integral of $pn(p)$. The extra factor of p in the integrand suppresses the effects due to the condensate-induced singularity at small p. For this reason, the presence of the condensate-induced singularity has little effect on the extraction of $R(Y,Q)$ from our scattering data.

In principle, the same procedure as used above could be used to determine FSE broadening in the normal liquid. However, due to the limited statistical accuracy of the data (3%) and the small effect of FSE's in the normal liquid as shown in Fig. 3(a), it is not possible to extract a final-state broadening function using the same procedure as for the superfluid. The experimental data must posses much higher statistical accuracy before a broadening function can be determined experimentally in the normal liquid.

There is a possible point of confusion regarding the FSE's in the normal fluid which we wish to clarify. The fact that FSE's appear to have little effect for the normal-fluid data does not necessarily mean that the FSE broadening function for the normal fluid is significantly different from that for the superfluid. In fact, if the physical ideas behind the successful FSE broadening theory of Silver[12] (discussed in Sec. V) are correct, then one would expect the broadening function for the normal fluid to differ little from that of the superfluid. At this point, we merely wish to point out that there is no internal inconsistency in this possibility. Since the scattering in the normal fluid is nearly Gaussian and the extracted FSE broadening function in the superfluid is relatively narrow by comparison and has zero second moment, the shapes of the broadened and unboardened distributions for the normal fluid would be almost indistinguishable.

We can also determine the form of FSE deviations from the point of view of the additive theories. To obtain the corrections to the IA result for this case, the theoretical prediction using the IA must be subtracted from the measured scattering after the instrumental broadening has been removed. For perfect data with no statistical noise, a unique deconvolution is possible. However, for data with statistical noise, deconvolution is an ill-posed problem which can lead to large and unphysical fluctuations in the results. Therefore, in the presence of statistical noise, a whole family of scattering functions can provide an accurate description of the observed scattering.

Rather than attempt to deconvolute the instrumental resolution, we will fit a model function broadened by the instrumental resolution to the observed scattering. We will choose the model such that is has physically realistic behavior and sufficient flexibility to accurately reflect the behavior of the true scattering. The model scattering function that we have found most convenient for describing the observed scattering is a sum of Gaussians:

$$J_{\text{model}}(Y)=\sum_{i=1}^{n}\frac{a_i}{(2\pi\sigma_i^2)^{1/2}}\exp\left[\frac{-(Y-Y_c)^2}{2\sigma_i^2}\right], \qquad (4.1)$$

whose amplitudes, widths, and common center may be varied. This form is not unique, and many other forms could be used to fit the data. Nevertheless, this form, with the restrictions that the amplitudes are always positive and the centers are locked together, does provide a physically realistic model scattering function. It is symmetric about Y_c and positive definite. It is free of spurious oscillations and other obviously unphysical features

TABLE I. Two Gaussian fitting parameters, resolution and FSE deconvoluted.

Temperature (K)	A_1 (%)	σ_1 (Å^{-1})	A_2 (%)	σ_2 (Å^{-1})	Y_c (Å^{-1})
0.35	0.785	0.95	0.215	0.29	−0.03
3.5	0.875	1.00	0.125	0.45	−0.04

which often appear when a direct deconvolution is attempted. The variation of the center of the scattering function Y_c enables the fitting function to take into account a scattering component which is asymmetric about $Y=0$ if such a component is present.

We have performed two Gaussian fits to the scattering data for both 0.35- and 3.5-K data. Excellent agreement with the observed scattering can be obtained at both temperatures using only two Gaussians in the model scattering function. The parameters used in the fitting functions are listed in Tabel I. Once again, we emphasize that the particular values of these parameters are only representative of an entire family of values which can equally well characterize the data. The widths and amplitudes of the fitted Gaussians are highly correlated, and a relatively broad set of parameters can lead to essentially the same shape for the underlying momentum distribution. The relative uncertainty of the scattering data is larger at high $|Y|$ due both to the lower counting statistics and the poorer signal-to-noise ratio. As a result, the $J_{\text{model}}(Y)$ scattering functions ar more tightly constrained by the data at small $|Y|$ than at large $|Y|$.

Armed with $J_{\text{model}}(Y)$, we can obtain the additive deviations due to FSE's for the normal and superfluid phases by subtracting $J_{\text{model}}(Y)$ from $J_{\text{IA}}(Y)$. The symmetric and antisymmetric components of $J_{\text{model}}(Y)$ for both the normal and superfluid phases are shown in Figs. 7(a) and 7(b), and the symmetric and antisymmetric correction terms $\Delta J_{\text{sym}}(Y,Q)$ and $\Delta J_{\text{asym}}(Y,Q)$ are shown in Figs. 7(c) and 7(d).

The corrections to the IA in the normal liquid obtained using $n(p)$ from the PIMC calculations of Ceperley and Pollock[5] are shown in Fig. 7(c). Both the symmetric and antisymmetric corrections are small. The maximum amplitude of the corrections is on the order of 5% of the total peak amplitude, comparable to the statistical accuracy of the data. The small size of the corrections is not surprising, given the good agreement of the IA prediction and the observed scattering shown in Fig. 3(a).

The corrections to the IA in the superfluid obtained using the $n(p)$ from the GFMC calculations of Whitlock and Panoff[4] are shown in Fig. 7(d). Both the symmetric and antisymmetric correction terms are now much larger than in the normal liquid. The maximum amplitude of the antisymmetric correction is now $\approx 20\%$ of the total peak amplitude, compared to $\approx 5\%$ in the normal liquid. The symmetric correction has a peak amplitude of $\approx 25\%$ of the total peak amplitude. In addition, it contains a negative δ-function singularity containing 9.2% of the total intensity. This term is required to cancel the condensate δ function in $J_{\text{IA}}(Y)$.

It is important to realize that this conclusion is unaffected even if one allows $J_{\text{model}}(Y)$ to include a narrow feature. If it were possible to include a sizeable narrow component in the fitting function, then it might be possible to significantly decrease the symmetric component of the difference. We have fit the superfluid data with a $J_{\text{model}}(Y)$ which includes a Gaussian much narrower than the instrumental resolution function. The narrow Gaussian in this fit reaches a size with only $\approx 1\%$ of the total area, which is close to the uncertainty with which the data determine the condensate. Even in this case, the symmetric component of the difference is almost a large as it is using the $J_{\text{model}}(Y)$ shown in Fig. 7(b).

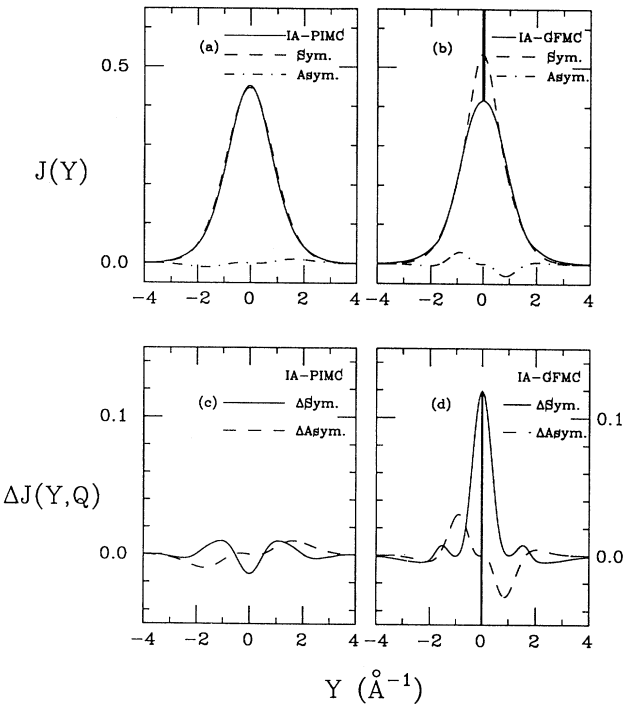

FIG. 7. (a) and (b) Comparisons of the IA predictions in the normal and superfluid phases with the model scattering function $J_{\text{model}}(Y)$ obtained from a fit to the data. The components of $J_{\text{model}}(Y)$ symmetric and antisymmetric about the recoil peak at $Y=0$ are plotted separately. (c) and (d) Symmetric and antisymmetric components of the additive correction for FSE's in the normal-fluid and superfluid phases.

The sum rules for incoherent scattering place restrictions on the shape of the symmetric and antisymmetric corrections to the IA which are recorded in Sec. II. It is not difficult to see that the experimentally determined $\Delta J_{\text{sym}}(Y,Q)$ and $\Delta J_{\text{asym}}(Y,Q)$ are consistent with these constraints. $\Delta J_{\text{asym}}(Y,Q)$ possesses two maxima and two minima as a function of Y, and $\Delta J_{\text{sym}}(Y,Q)$ has more than the minimum requirement of three extrema.

The reason for the appearance of a large positive component and a negative δ function in the symmetric correction term should be clear. The observed scattering contains no feature with a width comparable to the instrumental resolution. Therefore, the δ-function singularity due to the condensate in $J_{\text{IA}}(Y)$ must be removed and replaced with a broadened peak. This is a natural consequence of expressing the corrections to the IA as additive terms in the superfluid.

V. COMPARISON TO THEORIES

We now turn to an evaluation of FSE theories. Theoretical calculations for FSE may be tested by direct comparison to the observed scattering. The same pro-

cedure used in Sec. IV will be applied. The theoretical calculations for $n(p)$ are used to obtain the scattering in the IA. The results are then corrected for FSE's, using the appropriate theory, and broadened by instrumental resolution function. These results may then be compared directly to the observed scattering to evaluate the theories.

A number of theories predict a Lorentzian form for the FSE broadening function over most or all of the Y range. The earliest estimate of FSE's in liquid ^{4}He, by Hohenberg and Platzman,[28] takes the form of a convolution in which the broadening function is a Lorentzian:

$$R(Y,Q)=\frac{1}{\pi}\frac{\Gamma(Q)}{Y^2+\Gamma(Q)^2} . \tag{5.1}$$

The width used for the FSE broadening was $\Gamma(Q)=\rho\sigma(Q)$, where ρ is the density and $\sigma(Q)$ is the total cross section for helium atom-atom scattering. More recent Lorentzian theories obtain a width of $\Gamma(Q)=\rho\sigma(Q)/2$, half the size of the original Hohenberg-Platzman value. These theories include the asymmetric Lorentzian obtained by Platzman and Tzoar,[29] the Lorentzian calculated by Reiter and Becher[30] in a quasiclassical approximation, and the result of Kirkpatrick[31] which is approximately Lorentzian near $|Y|=0$.

Figure 4 shows the Lorentzian broadening for the experimental conditions of this work using the smaller value of $\rho\sigma(Q)/2$ for the width. Figure 8(a) and 8(b) show a comparison of the theoretical and experimental results in both the normal and superfluid phases. In both cases, the broadening is far larger than that observed experimentally. The theoretical results are not in agreement with the experimental observations using a Lorentzian broadening function of this width.

There is a theoretical objection to any broadening function with a Lorentzian form. A Lorentzian function possesses an infinite second moment and is therefore in violation of the second-moment sum rule for incoherent scattering discussed in Sec. II. However, the high-Y region of the Lorentzian function which is responsible for its finite second moment is not tightly constrained by the high-Y tails of the scattering data. Thus this theoretical objection does not preclude a strong constraint on the form of the broadening function extracted from the experimental data.

The failure of the existing Lorentzian theories for FSE's is chiefly due to the size of the predicted width and not their Lorentzian form. With an appropriate choice for the width, it is possible to obtain good agreement with the data using a Lorentzian broadening function or even a Gaussian broadening function. The main feature of the FSE broadening function which is constrained by the data is its width.

From the point of view of some more recent FSE broadening theories, there is a physical reason why Lorentzian theories overestimate the broadening.[32] The Lorentzian form for the broadening follows from the assumption that the struck He atom scatters from the other atoms in the liquid at a rate which is independent of the distance of the recoiling atom from the point of collision. In reality, however, this scattering rate is not constant as

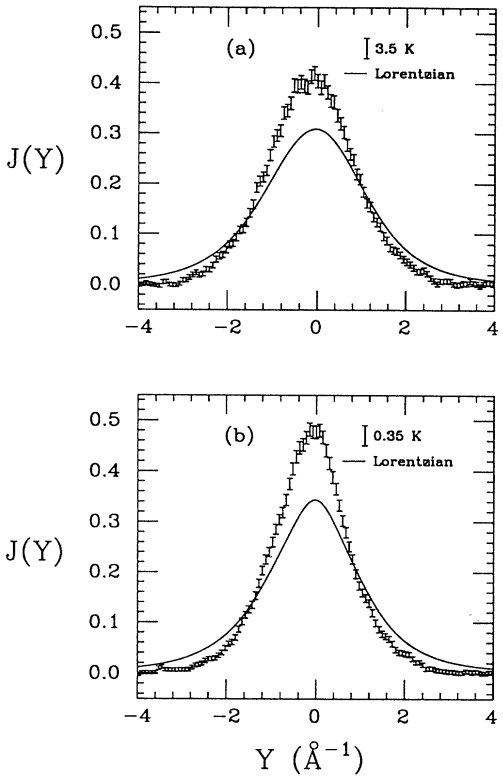

FIG. 8. (a) and (b) Comparison of the observed scattering with the theoretical prediction, converted to $J(Y)$ and broadened by instrumental resolution, using the Lorentzian broadening function of Hohenberg and Platzman with a width $\Gamma=\rho\sigma(Q)/2$.

a result of the strong correlations among the atoms in the liquid which are present before the atom is struck. Since the mean separation between the He atoms places them outside of the hard-core region of the potential responsible for the final-state scattering, the real scattering rate at small times (and therefore at large Y) is lower than that derived from the Lorentzian theories. By taking interparticle correlations among the atoms into account, these theories can be made consistent with the second-moment sum rule and can result in a broadening function with a narrower width.

Gersch and Rodriguez[33] made the first explicit attempt to include the effects of ground-state correlations within this approach. As a result, they obtained a final-state broadening which is not Lorentzian. Instead, it contains both a central peak which is narrower than that of the Lorentzian theories and negative tails. The Gersch-Rodriguez theory is consistent with the second-moment sum rule. The calculated broadening is shown in Fig. 4. Figures 9(a) and 9(b) show a comparison of the predicted and observed scattering. The agreement in the normal liquid is excellent. In the superfluid phase, the predicted intensity at the peak is slightly too high. Nevertheless, the agreement of the Gersch-Rodriguez theory with experiment is quite impressive.

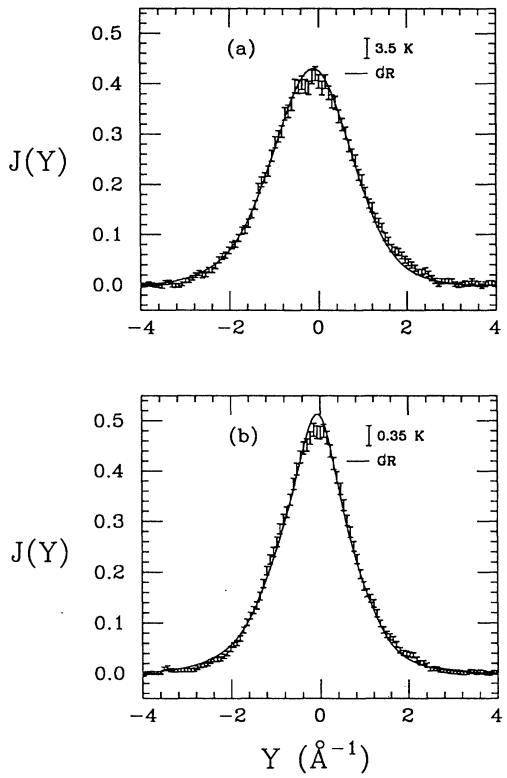

FIG. 9. (a) and (b) Comparison of the observed scattering with the theoretical prediction, converted to $J(Y)$ and broadened by instrumental resolution, using the broadening function calculated by Gersch and Rodriguez.

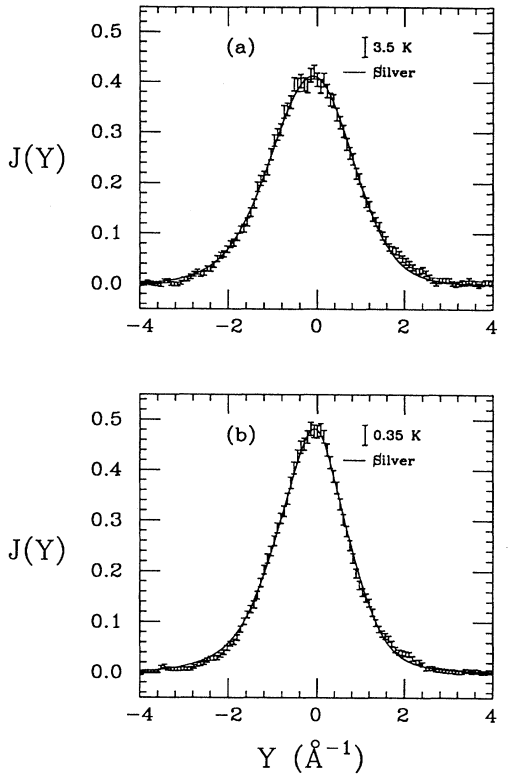

FIG. 10. (a) and (b) Comparison of the observed scattering with the theoretical prediction, converted to $J(Y)$ and broadened by instrumental resolution, using the broadening function calculated by Silver.

Most recently, Silver[12] has calculated a broadening function similar to that of Gersch and Rodriguez (GR). The physical point of view taken in Silver's theory is similar to that of Gersch and Rodriguez, but there are a number of differences in detail. Silver uses improved approximations for the two-body t matrix at high Q (semiclassical versus eikonal approximations), uses different approximations for the two-body density matrix which satisfy sum rules, and expresses the theory in terms of the Y-scaling variables. Silver's theory also uses more accurate inputs which were unavailable at the time of GR's work, such as the experimentally measured $g(r)$ instead of a step function approximation to $g(r)$ and more accurate He-He potentials as measured by He-He scattering experiments. A detailed comparison between various theories for FSE's has been performed by Silver.[34] The most important difference is that the GR theory uses a longer classical trajectory before collisions begin than Silver's theory (as illustrated in Ref. 34, Fig. 4), and this is the reason why FSE's are smaller in the GR theory than in Silver's theory.

The broadening function calculated by Silver for the experimental conditions used in this measurement is shown in Fig. 4. A comparison of the predicted and observed scattering using Silver's theory is shown in Figs. 10(a) and 10(b). The agreement is excellent in both the superfluid and normal-liquid phases at this Q. There are deviations between Silver's broadening function and the experimentally determined broadening function for $|Y|>0.8$ Å^{-1}, but since the data do not tightly constrain the form of $R(Y,Q)$ for large $|Y|$ these differences are not particularly significant. The main reason for the success of Silver's theory from an experimental point of view is that the width of the broadening function agrees with that extracted from experiment.

In another large class of FSE theories, the additive theories, deviations from the IA are expressed as additive corrections to the IA result. These corrections are then split into terms that are either symmetric or antisymmetric about $Y=0$. One of the reasons for the interest in this approach to FSE corrections is that if the antisymmetric correction is dominant, then most of the FSE's can be removed from the experimental data by simply symmetrizing the data. In addition, since the removal of the antisymmetric term leaves both the zeroth and second moment for incoherent scattering unchanged, this procedure has no effect on any determination of the average kinetic energy using the second-moment sum rule.

Sears[35] performed a formal expansion of the Compton profile $J(Y,Q)$:

$$J(Y,Q)=J_{\mathrm{IA}}(Y)+\sum_{n=3}^{\infty}(-1)^n A_n(Q)\frac{d^n}{dY^n}J_{\mathrm{IA}}(Y)\ , \tag{5.2}$$

in terms of $J_{IA}(Y)$ and it derivatives with coefficients depending on Q. The leading-order correction to $\Delta J_{asym}(Y,Q)$ was found to be of order $1/Q$, and the leading-order correction to $\Delta J_{sym}(Y,Q)$ was found to be of order $1/Q^2$. If this is true, then the antisymmetric correction should be much larger than the symmetric correction. Sears noted that this expansion would not be valid for superfluid helium due to the presence of the condensate. There is no reason, however, for it to fail in the normal fluid.

To test this expectation, we return to the decomposition of the symmetric and antisymmetric contributions to FSE's extracted in Sec. IV. In the normal liquid, as shown in Fig. 7(c), both the symmetric and antisymmetric corrections are small. Unfortunately, the corrections are so small that no conclusions can be drawn regarding which correction is dominant. The fact that the corrections are small is not inconsistent with the symmetrization prediction. The symmetrization treatment of FSE corrections does not modify the second moment of the data. Thus it will have little effect on the broad, nearly Gaussian momentum distribution in the normal fluid.

In the superfluid, as shown in Fig. 7(d), the symmetric and antisymmetric corrections are much larger than in the normal fluid. In addition, the symmetric correction is larger than the antisymmetric correction. The symmetric correction consists of a negative δ-function singularity with 9.2% of the total intensity superimposed on a net positive part with a peak amplitude of approximately 25% of the total peak amplitude. [The negative δ function is required to cancel the condensate δ function which appears in $J_{IA}(Y)$.] Symmetrization does not remove the dominant part of FSE's.

Another approach to the description of FSE's in liquid ^{4}He attempts to incorporate some of the effects of interparticle interactions, not in the form of a broadening function, but into the definition of the Y scale itself. Theoretical predictions using an alternative Y scale have been made by Stringari,[36] and the general approach has recently been described by Mayers.[37] (Strictly speaking, this shift should be referred to as an initial-state effect rather than a final-state effect, since it arises from an attempt to account for the change in the initial energy of the atom due to its binding in the condensed phase.) Such a description is incapable of describing the broadening of the condensate peak observed in the experimental studies.

Stringari predicts that the recoil peak should be shifted below the IA prediction of $Y=0$ by $M_{He}E_k/Q$ (E_k is the average kinetic energy). The predicted peak shift of -0.11 Å^{-1} is not apparent in the scattering data at $Q=23$ Å^{-1}. The approximations underlying the Stringari model have been criticized by Rinat as too drastic.[38] Nevertheless, it is possible that the use of a different Y-scaling, variable may be useful in describing the antisymmetric component of FSE corrections at lower values of Q.

Finally, a new calculation of FSE's which makes use of an alternative Y variable has been performed by Rinat and Taragin.[39] Rinat and Taragin expand the Compton profile $J(Y_R,Q)$ in a power series in M_{He}/Q with coefficients depending on Q and an alternative Y variable Y_R. The difference between Y_R and Y is of order $1/Q$ and thus vanishes in the $Q\rightarrow\infty$ limit. Figure 11 shows a comparison performed by the authors of their theory with the $Q=23$ Å^{-1} data in terms of the West Y variable used throughout this paper. The comparison shows good agreement in the normal-liquid phase. In the superfluid phase, the theoretical prediction of Rinat and Taragin is narrower than the experimental data near $Y=0$.

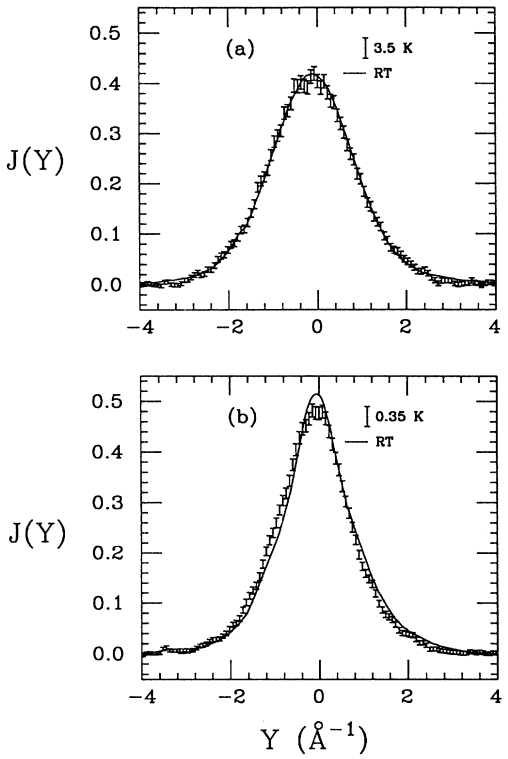

FIG. 11. (a) and (b) Comparison of the observed scattering with the theoretical prediction, converted to $J(Y)$ and broadened by instrumental resolution, using the additive FSE theory of Rinat and Taragin.

VI. CONCLUSIONS

We have carried out a test of theories for final-state effects in liquid ^{4}He by comparing the observed scattering in the normal and superfluid phases of liquid ^{4}He with theoretical predictions for the scattering, using current calculations for the momentum distribution as input. Therefore, implicit in our test is the assumption that the theoretical calculations of the momentum distribution are accurate. Obviously, our conclusions regarding FSE's are accurate only to the extent that the theoretical calculations are accurate.

We find that several of the theories for FSE's are consistent with the scattering observed in the normal-liquid phase in which $n(p)$ is broad and featureless. The only theories which fail in the normal liquid are those that predict Lorentzian broadening with a width $\rho\sigma/2$. These theories predict a scattering that is much broader than

that observed experimentally.

The scattering in the superfluid phase provides a much more stringent test for FSE theories due to the presence of the condensate. In the superfluid phase, only Silver's theory provides an accurate description of the FSE's. The theory of Gersch and Rodriguez also produces fair agreement. From the point of view of the additive theories, the data indicate that the symmetric correction is larger than the antisymmetric correction.

However, the success of the Silver's theory for the single momentum transfer of 23 Å^{-1} used in this experiment does not by any means imply that the problem of FSE's in liquid ^{4}He is solved. Recent calculations of the two-body density matrix in liquid ^{4}He give results which are significantly different from the approximation used in Silver's theory.[40] Whether or not these differences significantly modify Silver's prediction remains to be seen. For lower values of Q where most of the experimental data exist, Silver's theory may not apply in its present form at all.

Much experimental work remains to be done to clarify the nature of FSE's in liquid ^{4}He. In particular, it would be very interesting to extend the measurements performed at $Q = 23$ Å^{-1} to lower values of Q, both to determine where Silver's theory fails and to make contact with the previous lower-Q experiments. Experiments in both the normal and superfluid should be performed, since any differences between the two phases in the Q dependence of FSE's could give important insight into the underlying physics. If more theoretical calculations of momentum distributions are performed at higher densities, then it would also be possible to perform quantitative experiments to investigate the density dependence of FSE's.

ACKNOWLEDGMENTS

This work was supported by NSF Grant No. DMR-8704288 and OBES/DMS of the Intense Pulsed Neutron Source at Argonne National Laboratory under DOE Grant No. W-31-109-ENG-38. R.N.S. acknowledges OBES/DMS support of the Los Alamos Neutron Scattering Center. T.R.S. and W. M.S. acknowledge the support of the Division of Educational Programs at Argonne National Laboratory.

*Present address: Life Sciences Division, Los Alamos National Laboratory, Los Alamos, NM 87545.

†Present address: Quantum Metrology Group, National Institute of Standards and Technology, Gaithersburg, MD.

[1]An overview of such measurements can be found in *Momentum Distributions,* edited by R. N. Silver and P. E. Sokol (Plenum, New York, 1989).

[2]G. B. West, Phys. Rep. C **18**, 263 (1975).

[3]G. B. West (unpublished).

[4]P. A. Whitlock and R. Panoff, Can. J. Phys. **65**, 1409 (1987).

[5]D. M. Ceperley and E. L. Pollock, Can. J. Phys. **65**, 1416 (1987).

[6]E. Manousakis and V. R. Pandharipande, Phys. Rev. B **31**, 7029 (1985).

[7]E. L. Pollock and D. M. Ceperley, Phys. Rev. B **36**, 8343 (1987).

[8]R. A. Cowley and A. D. B. Woods, Can. J. Phys. **49**, 177 (1971).

[9]H. A. Mook, Phys. Rev. Lett. **32**, 1167 (1974).

[10]H. A. Mook, R. Scherm, and M. K. Wilkinson, Phys. Rev. A **6**, 2268 (1972).

[11]P. Martel, E. C. Svensson, A. D. B. Woods, V. F. Sears, and R. A. Cowley, J. Low Temp. Phys. **23**, 285 (1976).

[12]R. N. Silver, in *Proceedings of the 11th International Workshop on Condensed Matter Theories, Oulu, Finland,* edited by J. S. Arponen, R. F. Bishop, and M. Manninen (Plenum, New York, 1987), Vol. 3, p. 131; Phys. Rev. B **37**, 3794 (1988); **38**, 2283 (1988); **39**, 4022 (1989).

[13]S. W. Lovesey, *Theory of Neutron Scattering from Condensed Matter* (Oxford University Press, New York, 1984), Vol. I, Chap. 3.

[14]E. C. Svensson, V. F. Sears, A. D. B. Woods, and P. Martel, Phys. Rev. B **21**, 3638 (1980).

[15]A. Rahman, K. S. Singwi, and A. Sjölander, Phys. Rev. **126**, 986 (1962).

[16]J. J. Weinstein and J. W. Negele, Phys. Rev. Lett. **49**, 1016 (1982).

[17]P. E. Sokol, Can. J. Phys. **65**, 1393 (1987).

[18]W. G. Stirling, E. F. Talbot, B. Tanatar, and H. R. Glyde, J. Low Temp. Phys. **73**, 33 (1988).

[19]T. R. Sosnick, W. M. Snow, P. E. Sokol, and R. N. Silver, Europhys. Lett. **9**, 707 (1989).

[20]T. R. Sosnick, W. M. Snow, and P. E. Sokol, Phys. Rev. B **41**, 11 185 (1990).

[21]J. Gavoret and P. Nozières, Ann. Phys. (N.Y.) **28**, 349 (1964).

[22]G. Baym, in *Mathematical Methods in Solid State and Superfluid Theory,* edited by R. C. Clark and G. H. Derrick (Oliver and Boyd, Edinburgh, 1969).

[23]P. C. Hohenberg and P. C. Martin, Phys. Rev. Lett. **12**, 69 (1964).

[24]N. N. Bogoliubov, *Lectures on Quantum Statistics* (MacDonald Technical and Scientific, London, 1970), Vol. 2.

[25]A. Griffin, Phys. Rev. B **30**, 5057 (1984).

[26]A. Griffin, Phys. Rev. B **32**, 3289 (1985).

[27]*Momentum Distributions,* edited by R. N. Silver and P. E. Sokol (Plenum, New York, 1989), p. 143.

[28]P. C. Hohenberg and P. M. Platzman, Phys. Rev. **152**, 198 (1966).

[29]P. M. Platzman and N. Tzoar, Phys. Rev. B **30**, 6397 (1984).

[30]G. Reiter and T. Becher, Phys. Rev. B **32**, 4492 (1985).

[31]T. R. Kirkpatrick, Phys. Rev. B **30**, 1266 (1984).

[32]R. N. Silver, in *Proceedings of the 11th International Workshop on Condensed Matter Theories, Oulu, Finland* (Ref. 12).

[33]H. A. Gersch and L. J. Rodriguez, Phys. Rev. A **8**, 905 (1973); L. J. Rodriguez, H. A Gersch, and H. A. Mook, *ibid.* **9**, 2085 (1974).

[34]R. N. Silver, Phys. Rev. B **38**, 2283 (1988).

[35]V. F. Sears, Phys. Rev. B **30**, 44 (1984).

[36]S. Stringari, Phys. Rev. B **35**, 2038 (1987).

[37]J. Mayers, Phys. Rev. B **41**, 41 (1990).

[38]A. S. Rinat, Phys. Rev. B **36**, 5171 (1987).

[39]A. S. Rinat and M. F. Taragin, Phys. Rev. B **41**, 4247 (1990).

[40]M. L. Ristig and J. W. Clark, Phys. Rev. B **40**, 4355 (1989).